

THE GENESIS OF THE MILKY WAY'S THICK DISK VIA STELLAR MIGRATION

SARAH R. LOEBMAN¹, ROK ROŠKAR¹, VICTOR P. DEBATTISTA^{2,3}, ŽELJKO IVEZIĆ^{1,4}, THOMAS R. QUINN¹, AND JAMES WADSLEY⁵

Draft version November 9, 2018

ABSTRACT

The separation of the Milky Way disk into a thin and thick component is supported by differences in the spatial, kinematic and metallicity distributions of their stars. These differences have led to the predominant view that the thick disk formed early via a cataclysmic event and constitutes fossil evidence of the hierarchical growth of the Milky Way. We show here, using N -body simulations, how a double-exponential vertical structure, with stellar populations displaying similar dichotomies can arise purely through internal evolution. In this picture, stars migrate radially, while retaining nearly circular orbits, as described by Sellwood & Binney (2002). As stars move outwards their vertical motions carry them to larger heights above the mid-plane, populating a thickened component. Such stars found at the present time in the solar neighborhood formed early in the disk's history at smaller radii where stars are more metal-poor and α -enhanced, leading to exactly the properties observed for thick disk stars. Classifying stars as members of the thin or thick disk by either velocity or metallicity leads to an apparent separation in the other property as observed. This scenario is supported by the SDSS observation that stars in the transition region do not show any correlation between rotational velocity and metallicity. Although such a correlation is present in young stars because of epicyclic motions, the radial migration mixes stars, washing out the correlation. Using the Geneva Copenhagen Survey, we indeed find a velocity-metallicity correlation in the younger stars and none in the older stars. We predict a similar result when separating stars by $[\alpha/\text{Fe}]$. The good qualitative agreement between our simulation and observations in the Milky Way are especially remarkable because the simulation was not tuned to reproduce the Milky Way, hinting that the thick disk may be a ubiquitous galaxy feature generated by stellar migration. Nonetheless, we cannot exclude that some fraction of the thick disk is a fossil of a past more violent history, nor can this scenario explain thick disks in all galaxies, most strikingly those which counter-rotate with respect to the thin disk.

Subject headings: galaxies: evolution — galaxies: spiral — galaxies: stellar content — Galaxy: solar neighborhood — Galaxy: stellar content — stellar dynamics

1. INTRODUCTION

In the years since Gilmore & Reid (1983) first proposed a two component structure to the Milky Way disk, a large body of observational work has provided supporting evidence for contrasting thin and thick disk attributes. Structurally, the thin disk scale height is shorter than thick disk scale height (for reviews see Majewski 1993; Buser et al. 1999; Norris 1999, and references therein), and the thick disk may have a longer scale length than the thin disk (Robin et al. 1996; Ojha 2001; Chen et al. 2001; Larsen & Humphreys 2003). Kinematically, thick disk stars have larger velocity dispersions and lag the net rotation of the disk (Nissen 1995; Chiba & Beers 2000; Gilmore et al. 2002; Soubiran et al. 2003; Parker et al. 2004; Wyse et al. 2006). Additionally, thick disk stars are older and metal poor relative to their thin disk counterparts (*e.g.* Majewski 1993; Chiba & Beers 2000; Bochanski et al. 2007) and at a given iron abundance thick disk stars are α -enhanced (Fuhrmann

1998; Prochaska et al. 2000; Tautvaišienė et al. 2001; Bensby et al. 2003; Feltzing et al. 2003; Mishenina et al. 2004; Brewer 2004; Bensby et al. 2005). Moreover, thin and thick disk attributes are not unique to the Milky Way but a ubiquitous feature for late type galaxies (Burstein 1979; van der Kruit & Searle 1981; Abe et al. 1999; Neerer et al. 2002; Yoachim & Dalcanton 2005, 2006; Yoachim 2007).

Recently, several SDSS-based studies have provided further strong observational constraints on the structural, kinematic and chemical properties of stars in the solar cylinder. Jurić et al. (2008, hereafter J08) used a photometric parallax method on SDSS data to estimate distances to ~ 48 million stars and studied their spatial distribution. Because SDSS provides accurate photometry, which enables reasonably robust distances (10–15%, Sesar et al. 2008), as well as faint magnitude limits ($r < 22$) and a large sky coverage (6500 deg²), J08 were able to robustly constrain the parameters of a model for the global spatial distribution of stars in the Milky Way. The J08 model is qualitatively similar to previous work (*e.g.* Bahcall & Soneira 1980) which identifies a clear change of slope in the counts of disk stars as a function of distance from the Galactic plane; this change in slope is usually interpreted as the transition from the thin to thick disk (Gilmore & Reid 1983; Siegel et al. 2002).

Ivezić et al. (2008, hereafter I08) further extended this

¹ Astronomy Department, University of Washington, Box 351580, Seattle, WA 98195-1580, USA; sloebman@astro.washington.edu

² Jeremiah Horrocks Institute, University of Central Lancashire, Preston, PR1 2HE, UK; vpdebattista@uclan.ac.uk

³ RCUK Fellow

⁴ University of Zagreb, Croatia

⁵ Department of Physics and Astronomy, McMaster University, Hamilton, Ontario, L8S 4M1, Canada

global analysis of SDSS data by developing a photometric metallicity estimator and by utilizing a large proper motion catalog based on SDSS and Palomar Observatory Sky Survey data (Munn et al. 2004). I08 studied the dependence of the metallicity, $[\text{Fe}/\text{H}]$ and rotational velocity, V_ϕ , of disk stars on the distance from the Galactic plane and detected gradients of both quantities over the distance ranging from several hundred parsecs to several kiloparsecs. Such gradients would be expected in a thin/thick disk decomposition where the thick disk stars are a separate population defined by a bulk rotational velocity lag and a lower metallicity compared to those of the thin disk. However, such a model would also predict a correlation between the metallicity and the velocity lag, which is strongly excluded ($\sim 7\sigma$ level) by the I08 analysis (see Figure 17, I08). In this work we turn to a more sophisticated Galactic description — an N -body model — to characterize stars within the SDSS volume and solve this puzzle.

Over the past few decades, N -body simulations have been used to provide supporting evidence for three distinct theories of thick disk formation: violent relaxation (Jones & Wyse 1983), substructure disruption (Statler 1988), and heating by satellites (Quinn et al. 1993). Several works have recently redressed these ideas. Brook et al. (2004) and Bournaud et al. (2009) formed a thick disk in situ at high redshift during gas-rich mergers, where star formation is triggered by the rapid accretion of gas; this result is consistent with the thick disk forming through violent relaxation of the galactic potential. In contrast, Kazantzidis et al. (2008), Villalobos & Helmi (2008), and Villalobos et al. (2010) investigated substructure disruption by using a cosmologically derived satellite accretion history to perturb a Milky Way-like disk; subhalo-disk encounters increased the scale height of this disk at all radii effectively forming a thick disk. Finally, Abadi et al. (2003) showed that by tidally stripping/accreting satellites, the majority of the oldest stars in the thick disk could have formed externally rather than in situ.

In this work, we study a new method of formation: radial migration. Radial migration due to scattering from transient spirals was first described by Sellwood & Binney (2002). In this model energy and angular momentum changes occur from interactions with transient spiral arms, which move stars at the corotation resonance inward or outward in radius while preserving their nearly-circular orbits. Roškar et al. (2008a,b, R08ab hereafter) studied this phenomenon in N -body + Smooth Particle Hydrodynamic (SPH) simulations of disk formation, and showed that migrations are possible on short timescales. They explored the implications of radial mixing for stellar populations for a variety of stellar systems, including the solar neighborhood. Here we extend their work by highlighting the vertical evolution that occurs as a result of migration.

We note that in this paper, we are not testing the validity of the other models of formation. However, recently, Sales et al. (2009) proposed using the eccentricity of orbits of stars in the thick disk to constrain the thick disk’s formation mechanism; they presented the eccentricity distributions that result from four N -body simulations: Abadi et al. (2003), Villalobos & Helmi (2008), R08b, and Brook et al. (2004). They found that the

distributions that result from heating, radial migration and mergers all had a strong peak at low eccentricity ($\epsilon \sim 0.2 - 0.3$), while the distribution that results from accretion is centered at higher orbital eccentricities ($\langle \epsilon \rangle \sim 0.5$). Building on this, Wilson et al. (2010) studied the eccentricity of orbits of stars in the thick disk observed in the Radial Velocity Experiment (RAVE) (Steinmetz et al. 2006) and found these results to be inconsistent with expectations for the pure accretion simulation. Ruchi et al. (2010) also leveraged α measurements from RAVE to conclude that the α enhancement of the metal-poor thick disk implies that direct accretion of stars from dwarf galaxies did not play a major role in the formation of the thick disk. Using SDSS DR7, Dierickx et al. (2010) showed that the eccentricity of orbits of stars in the thick disk implies the thick disk is unlikely to be fully populated by radially migrated stars. We note that we cannot exclude that some fraction of the thick disk is a fossil of a past more violent history, nor can this scenario explain thick disks in all galaxies. However, in what follows, we show that a large fraction of the stars in the thick disk could have formed in situ and arrived at their present location via radial migration.

The outline of this paper is as follows: in §2, we present two simulations, one with substantial migration and the other with relatively little migration. When we compare these two simulations we can show that migration can build a thick disk as first conceived by Gilmore & Reid (1983): a component with a scale-height larger than that of the thin disk. In §3 we qualitatively compare the Milky Way-like simulation (with migration) with the SDSS observations to show that they match each other sufficiently well to pursue further comparison. In §4 we present a detailed comparison between the simulation and the local SDSS volume focusing on the reason for the lack of correlation between V_ϕ and $[\text{Fe}/\text{H}]$; in Appendix A we reconsider recent observational claims concerning the lack of correlation between V_ϕ and $[\text{Fe}/\text{H}]$. In §5 we use the simulation as a proxy for the Milky Way to show that classifying stars as members of the thin or thick disk by either velocity or metallicity leads to an apparent separation in the other property as observed. In §6 we compare our results to recent theoretical work that used semi-analytics to investigate how the solar neighborhood could have been shaped by radial migration and chemical evolution effects. In §7 we explore the correlation between $[\alpha/\text{Fe}]$ and age to show the diagnostic power of $[\alpha/\text{Fe}]$ as a stand-in for age. Finally, in §8 we summarize our results and conclusions.

2. NUMERICAL SIMULATIONS

We analyze the results of an N -body + SPH simulation designed to mimic the quiescent formation and evolution of a Milky Way-mass galaxy following the last major merger. The system is initialized as in Kaufmann et al. (2007) and R08ab and consists of a rotating, pressure-supported gas halo embedded in an NFW (Navarro et al. 1997) dark matter halo. This simulation was evolved for 10 Gyr using the parallel N -body+SPH code, GASOLINE (Wadsley et al. 2004). As the simulation proceeds, the gas cools and collapses to the center of the halo, forming a thin disk from the inside-out. Gas is continually infalling from the hot halo onto the disk for the duration of the simulation. Star

formation and stellar feedback are modeled with subgrid recipes as described in Stinson et al. (2006). Importantly, the stellar feedback prescriptions include SN II, SN Ia and AGB metal production, as well as injection of supernova energy which impacts the thermodynamic properties of the disk interstellar medium (ISM). Metal diffusion is calculated from a subgrid model of eddy turbulence based on the local smoothing length and velocity gradients (Smagorinsky 1963; Wadsley et al. 2008). The simulation we utilize is nearly identical to R08ab (see R08ab for further details), but with the addition of metal diffusion (Shen et al. 2009).

No *a priori* assumptions about the disk’s structure are made — its growth and the subsequent evolution of its stellar populations are completely spontaneous and governed only by hydrodynamics/stellar feedback and gravity. Although we do not account for the full cosmological context, merging in the Λ CDM paradigm is a higher order effect at the epochs in question (Brook et al. 2005). Thus, our model galaxy lacks some structural components such as a stellar halo, which in Λ CDM is built up primarily during the merging process (*e.g.* Bullock & Johnston 2005; Zolotov et al. 2009). Our focus here, however, is disk evolution; by simplifying our assumptions, we are able to use much higher resolution and more easily study the impact of key dynamical effects on observational properties of stellar populations within the disk.

Based on such simulations, R08ab presented the implications of stellar radial migration resulting from the interactions of stars with transient spiral arms (Sellwood & Binney 2002) on the observable properties of disk stellar populations. Radial migration efficiently mixes stars throughout the disk into the solar neighborhood, resulting in a flattened age-metallicity relation (R08ab). Figures 1, 2, & 3 illustrate the basic premise of this paper — stars migrate radially and in the process rise out of the plane over time, so many stars are presently not near their birth place. Previous studies have shown (Loebman et al. 2008; Sales et al. 2009; Caruana 2009; Schönrich & Binney 2009) that the vertical evolution that results from radial migration can influence the characterization of the thick disk.

In order to further illustrate the importance of radial migration within our adopted Milky Way (MW) simulation, we have repeated much of our analysis on a control case. The control simulation is a system with the same initial conditions as the MW simulation except for having a higher angular momentum content with a dimensionless spin parameter $\lambda = 0.1$ (Bullock et al. 2001). This results in a more extended disk (final disk scale-length = 5.04 kpc, versus 3.23 kpc for the MW simulation), possibly similar to a low surface brightness galaxy; we therefore refer to this simulation as the LSB simulation. Due to its lower surface density, the disk forms weaker spirals and as a result the stellar populations at all radii are less affected by radial mixing. When we compare migration as a function of scale-lengths, we find that there is significantly less migration in the LSB galaxy than in the MW galaxy.

The distribution of stellar mass away from the mid-plane is strongly affected by radial migration; this can be seen in Figure 4, which contrasts the MW simulation against the LSB case. Here the normalized mass den-

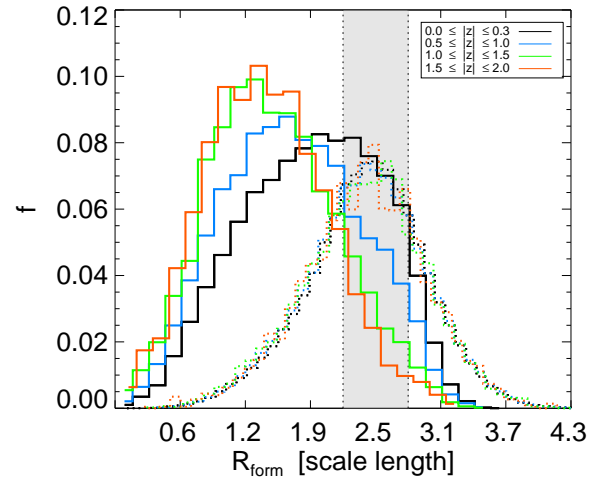


Figure 1. Star particles that fall within the solar cylinder at the end of the simulation are considered here. These stars are broken into four volumes by distance away from the mid-plane, $|z|$, with low to medium to high given by black to blue to red. For comparison, four similar volumes from the LSB simulation with little radial migration are over-plotted (dotted lines). For each volume, the formation radius of stars is shown; in the MW simulation, away from the mid-plane, a large fraction of the stars formed significantly interior to their final location. For reference, the solar cylinder is indicated in the shaded gray region: galactocentric radius = 2.2–2.8 scale lengths. In the MW simulation this corresponds to 7 kpc $\leq R \leq$ 9 kpc while in the LSB simulation it corresponds to 11 kpc $\leq R \leq$ 14 kpc.

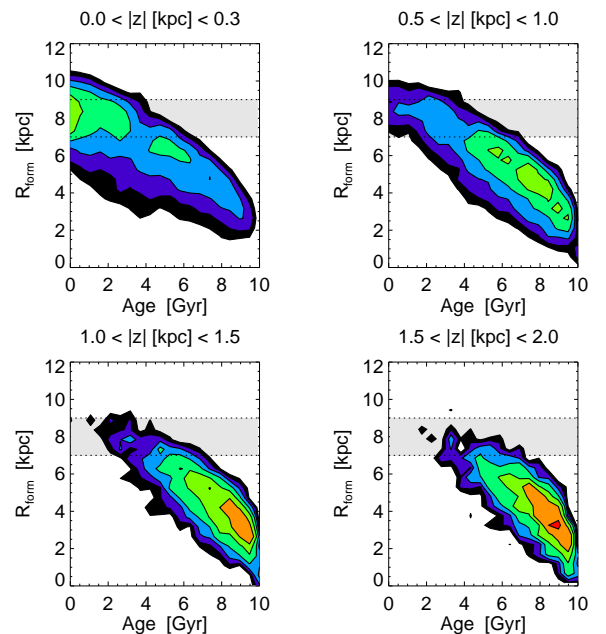


Figure 2. Contour plots of the MW simulation showing the distribution of R_{form} vs. Age for the four volumes considered in Figure 1 with solar cylinder shaded in gray. For all z , older stars formed significantly interior to their final location; this net outward movement of stars over time is due to radial migration. Volumes sampling the thick disk ($|z| \geq 1$ kpc) are dominated by older stars that have migrated to the solar radius from interior radii.

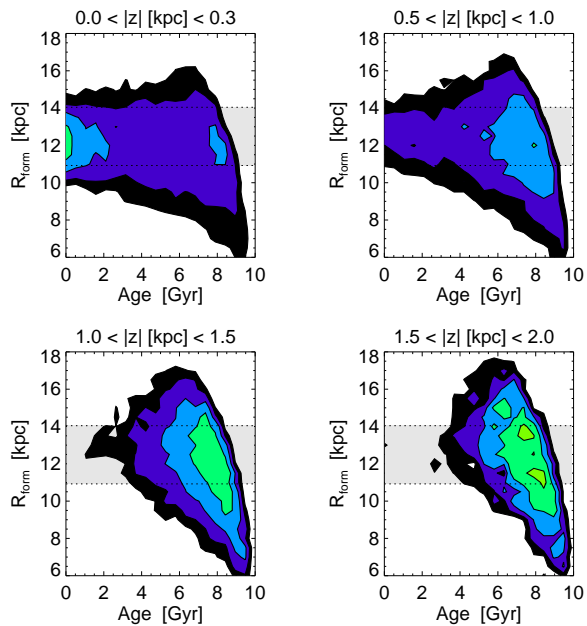


Figure 3. Same as Figure 2 but for the LSB simulation which has little radial migration. Regardless of distance away from the midplane, all stars originate from a roughly symmetric distribution centered at the midpoint of the cylindrical volume. While volumes sampling the thick disk ($|z| \geq 1$ kpc) are dominated by older stars, these stars are largely uninfluenced by radial migration.

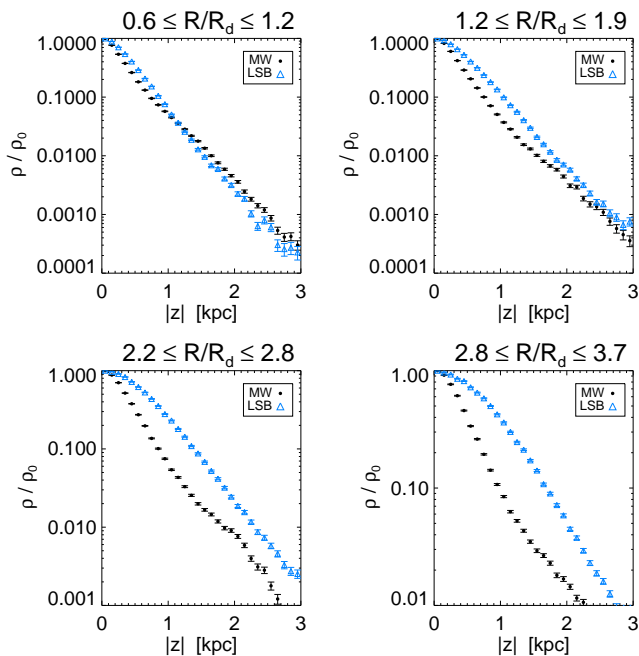


Figure 4. Density profiles drawn from analogous regions within the MW and LSB simulations. At larger radii, the LSB simulation has a fairly flat (pure exponential) profile whereas the MW simulation has a transition between a steep and shallow profile.

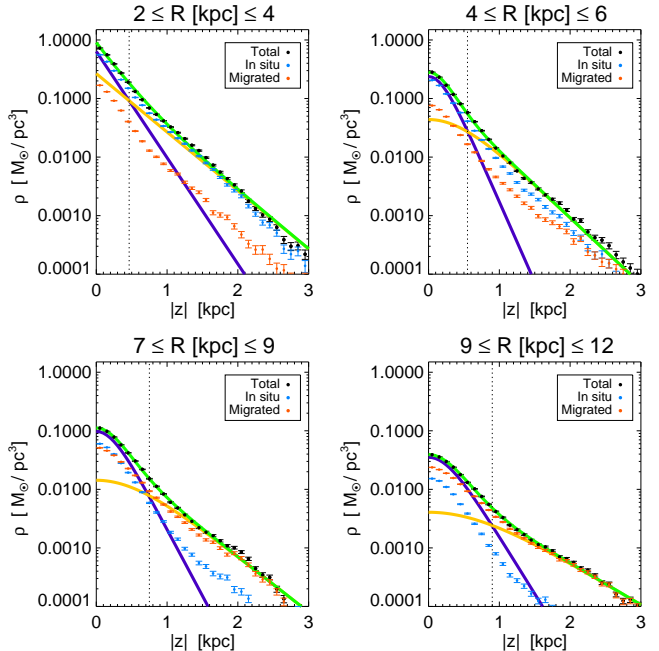


Figure 5. Simultaneous fits to the vertical density profile in the MW simulation for radial bins: $R = 2 - 4$ kpc, $R = 4 - 6$ kpc, $R = 7 - 9$ kpc, $R = 9 - 12$ kpc. While the radial bin sampling the smallest radii is best fit by a double exponential function, all other bins are better fit by a double sech² function. Best fit parameters are given in Table 1. Thin, thick, and total curves shown in purple, orange and green respectively; the vertical dotted line marks the intersection between thin and thick disk components. Red and cyan points represent stellar mass density that has migrated more than 2 kpc or less than 2 kpc respectively from radius of formation.

sity distribution within four analogous cylindrical volumes drawn from a variety of radii are presented. At larger radii, the steepness of the profiles are quite different; the LSB simulation has a constant slope while the MW simulation shows a transition from a steep to a shallow density distribution. Thus the MW simulation cannot be characterized by a single exponential or sech² component in the vertical direction, as we show explicitly in the following Section and Figure 5. It is this double-component nature which first led to the identification of the thick disk (Gilmore & Reid 1983); we have thus shown that this feature need represent nothing more than internal evolution of the Milky Way.

3. COMPARISON OF SIMULATIONS WITH SDSS

In the following section, we compare SDSS observations with the MW simulation to demonstrate its usefulness as a model for understanding the Milky Way thick disk. Here we study the stellar mass distribution, rotational velocity and metallicity as functions of distance from the Galactic plane, $|z|$, and galactocentric cylindrical radius, R . We draw qualitative comparisons between the datasets by examining their mass weighted metallicity and kinematic distributions in this R - $|z|$ space.

The observed Milky Way disk is best fit by a 2-component model that is exponential both in the R and z directions (see Table 10, bias-corrected results, J08). The top panel of Figure 6 shows the mass weighted density distribution of the entire MW simulation at its final timestep. This distribution is in qualitative agreement in both the R and z directions with J08 for up to ~ 2.5 kpc

R [kpc]	N1 [M_{\odot}/pc^3]	h1 [pc]	N2 [M_{\odot}/pc^3]	h2 [pc]
2 – 4	0.638	239	1.000	266
4 – 6	0.237	316	0.044	763
7 – 9	0.098	381	0.014	913
9 – 12	0.035	444	0.004	1197

Table 1

Best fit parameters to radial bins sampled in Figure 5 given by: thin disk normalization ($N1$), thin disk scale height ($h1$), thick disk normalization ($N2$), & thick disk scale height ($h2$).

above the disk’s plane and ~ 15 kpc from the galactic center.

Figure 5 shows our best fits to the vertical density profiles for the MW simulation for radial bins $R = 2 - 4$ kpc, $R = 4 - 6$ kpc, $R = 7 - 9$ kpc and $R = 9 - 12$ kpc. As in J08, the innermost radial bin is best fit by a double exponential function; however, all other bins are better fit by the sum of two double sech^2 profiles, which is in agreement with the theoretical work by Spitzer (1942) and observational results for other galaxies by Yoachim & Dalcanton (2006). Despite the small discrepancy between sech^2 vs. exponential fits, the simulation is in good qualitative agreement with the SDSS-based analysis of the Milky Way (J08).

In addition, Figure 5 shows the vertical density profiles as divided into two populations: radial migrators ($|R - R_{form}| > 2$ kpc) and an in situ population ($|R - R_{form}| \leq 2$ kpc). We note the second component fit for radial bins $R = 7 - 9$ kpc and $R = 9 - 12$ kpc is entirely dominated by star particles that have migrated. We expect that stars that moved from elsewhere combined with stars that were born locally should not naturally conspire to produce a single continuous profile.

For the solar cylinder, $R = 7 - 9$ kpc, we find that the model distribution of stars as a function of $|z|$ resembles a double sech^2 profile, with the “transition” height of $|z| \sim 0.75$ kpc, comparable to ~ 1 kpc found by J08 for the Galactic disk. We have found the best-fit scale heights to be 381 pc and 913 pc, in qualitative agreement with the best-fit scale heights of 270 pc and 1200 pc for the SDSS data (J08). The scale height ratio suggested by the simulation is slightly low — ~ 2.4 , instead of ~ 3 from the data. Moreover, the simulation’s thick disk to thin disk normalization is slightly discrepant — ~ 0.14 , rather than ~ 0.12 suggested by the SDSS data. Overall, we find that the thick disk in the MW simulation, formed through the process of radial migration, is qualitatively very similar to the observed Galactic thick disk. As Figure 4 clearly attests, this conclusion does not apply to the LSB simulation.

The median metallicity of the Milky Way disk exhibits a clear vertical gradient (see Figure 9, bottom two panels, I08). Notably, the spatial variation of the median metallicity does not follow the distribution of the stellar number density (I08). The middle panel of Figure 6 shows that the MW simulation reproduces a qualitatively similar metallicity distribution; we note that a constant additive offset of 0.2 dex has been applied to $[\text{Fe}/\text{H}]$ throughout the simulation so that the median metallicity in the plane of the disk in the solar cylinder matches observations. As expected, at low galactic latitudes and small radii, the volume is dominated by high (near solar) metallicities. At higher latitudes the volume is increas-

ingly metal poor.

As with metallicity, previous studies have found a gradient in the median V_{ϕ} with respect to z in the Milky Way (see Figures 5, 8, and 9 in Bond et al. (2010, hereafter B10), and references therein). These authors concluded that V_{ϕ} is also well characterized by a non-Gaussian distribution (see Binney 2010, for the implied distribution function). The bottom panel of Figure 6 shows that the MW simulation reproduces qualitatively similar V_{ϕ} properties, including a strong $|z|$ gradient.

Thus on a gross scale the MW simulation qualitatively matches patterns observed in mass density, metallicity and rotational velocity in the Milky Way disk. We now look at the solar cylinder in greater detail.

4. EFFECTS OF RADIAL MIGRATION ON THE SOLAR CYLINDER

4.1. Vertical Gradients

Here we study in detail the distributions of age, stellar mass, rotational velocity and metallicity as functions of $|z|$ for the solar cylinder. To be consistent with the analysis of high galactic latitude SDSS data by J08 and I08, we select model particles from an annulus with 7 kpc $\leq R \leq 9$ kpc. This radial cut spans 2.2–2.8 scale lengths from the center of model galaxy (scale length 3.2 kpc), and covers the Sun’s location of ~ 3 disk scale lengths from the Milky Way center (scale length ~ 2.6 kpc) (see bias-corrected value, Table 10, J08).

The behavior of the MW simulation in this particular volume is illustrated in Figure 7. The top panel shows the age distribution as a function of $|z|$. As expected, near the midplane, the population is dominated by young stars, and the mean age monotonically increases with increasing distance from the midplane. Only very old stars are found at large $|z|$: by $|z| \sim 0.5$ kpc the mean age is already ~ 5 Gyr. Recall that Figure 2 shows that with increasing distance from the midplane, the stellar population becomes dominated by older stars that formed closer to the center of the disk. These two figures taken together give a coherent picture of the net dynamic effect on the system: *on average stars move both radially outward and away from the midplane over time.*

Radial migration is able to change the extent of a star’s vertical oscillation, as a well as its rotational velocity (middle panel, Figure 7). In the MW simulation we find a vertical gradient of rotational velocity of -17 $\text{kms}^{-1}\text{kpc}^{-1}$ (compared to a gradient of -30 $\text{km s}^{-1}\text{kpc}^{-1}$ found by I08). Note that stars which significantly lag the rotation of the disk in the midplane have traditionally been regarded as members of the thick disk.

Another observed trend that is physically well motivated by the net outward and upward movement of stars over time is the decline of metallicity with increased height (bottom panel, Figure 7). In the MW simulation, the metallicity distribution changes with $|z|$ with a best-fit gradient of ~ 0.19 dex kpc^{-1} , again in qualitative agreement with the measured value for the Milky Way of ~ 0.30 dex kpc^{-1} (I08).

To understand how this trend arises, recall that the top panel of Figure 7 shows that the stellar population away from the plane is dominated by old stars. As Figure 2 shows, the oldest stars at large $|z|$ mostly formed in the inner 2 – 4 kpc. Moreover, at early times, the radial

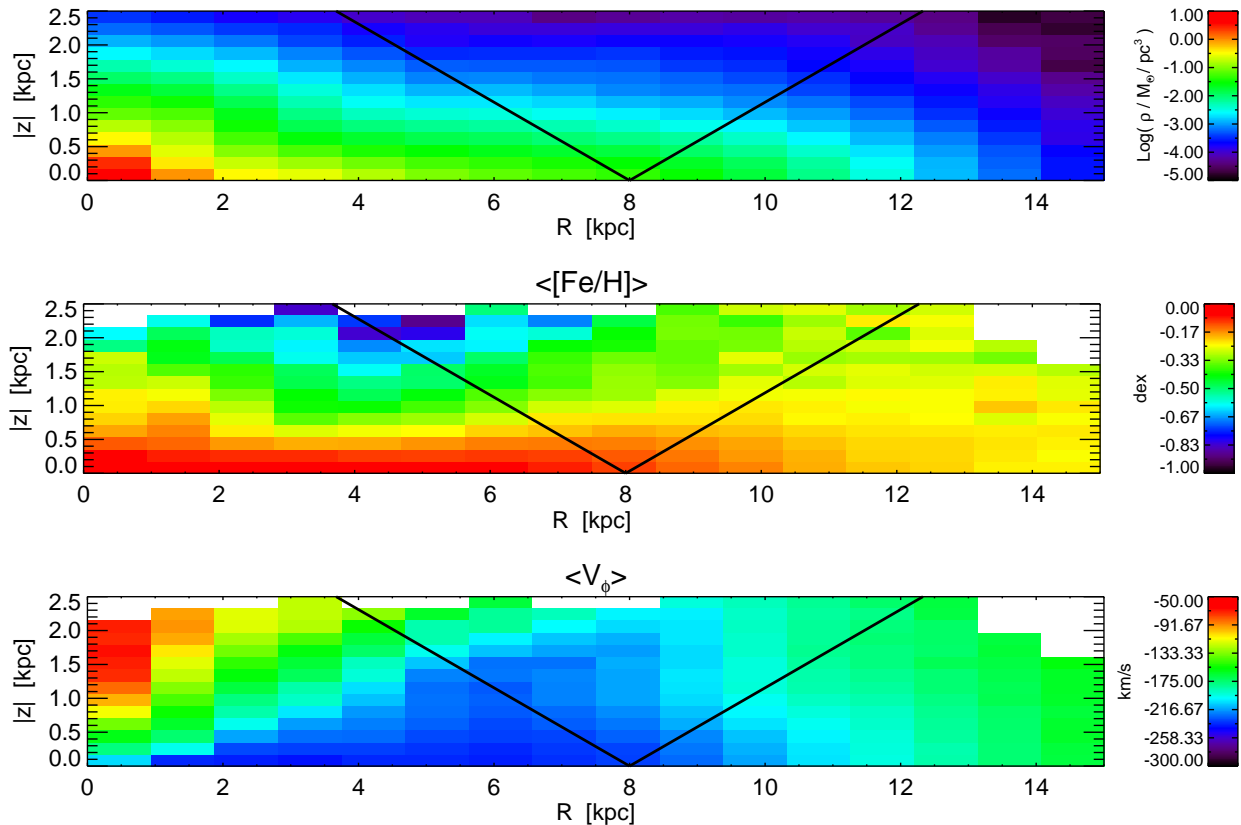


Figure 6. Top: Mass density distribution in galactocentric coordinates of the entire MW simulation. The colors scale logarithmically with density in each bin. Overplotted is the SDSS field of view ($|b| > 30^\circ$). Middle & Bottom: Mass-weighted mean $[\text{Fe}/\text{H}]$ and V_ϕ values as mapped onto the R - $|z|$ plane. For a color box to be plotted we required a minimum of 50 star particles.

metallicity gradient was steep (see Figure 2 in R08b); stars that are now in the thick disk in the solar cylinder in the MW simulation were once at the outer edge of the forming thin disk and hence formed at a low metallicity. As a result, stars that formed at a radius of 2–4 kpc early on in the galactic history are necessarily metal poor. These stars have been subsequently moved out and up over time. At later times, the metallicity gradient flattened out as the disk grew. Again, looking at Figure 1 (top right panel), one can see a significant fraction of young stars (*i.e.* less than 4 Gyr old) formed at $R \sim 6$ kpc where there was a relatively more metal rich ISM. These stars had less time to migrate and as a result remain closer to the midplane of the disk. This complex co-dependence of radial migration, birth location, and metallicity gradient evolution then gives rise to a vertical metallicity gradient in the solar neighborhood.

4.2. Thin/Thick Disk Transition

We turn our attention now to a particular region within the solar cylinder: $|z| = 0.5 - 1.0$ kpc, $R = 7 - 9$ kpc. This region in the simulation is analogous to the thin-thick disk “transition zone” considered by I08: within this volume a roughly equal number of thin and thick disk stars is expected (see bottom left panel, Figure 5). The transition region within the MW simulation occurs in approximately the same place as in the data (0.75 kpc versus ~ 1 kpc) which allows us to draw a direct comparison to the slice analyzed in I08. We show here that all the trends observed in the SDSS data can be

explained by a continuous distribution rather than two distinct populations.

In Figure 8 we show the distribution of observable properties as a function of age within this slice of the simulation. The top left panel of Figure 8 shows the distribution of ages in this thin volume slice: the region is well populated ($\sim 30,000$ star particles) and predominantly old (36% older than 7 Gyr, 63% older than 5 Gyr). The remaining panels in Figure 8 illustrate probability densities of formation radius, metallicity, and rotational velocity versus age. In all cases, the distributions do not suggest distinct populations. For the given $|z|$ slice, stars older than about 4 Gyr are both numerous and formed significantly interior to their present location (top right panel). These stars also show a rotational velocity lag of $\sim 20 \text{ km s}^{-1}$, as shown in the bottom left panel. The oldest stars, those with ages $\gtrsim 8$ Gyr, have significantly lower metallicities than younger stars (bottom right panel). And as noted previously, the oldest stars formed at a range of interior radii, when the ISM metallicity was low and had a steep radial gradient. These effects drive the behavior of various observables, as discussed next.

4.3. Rotational Velocity vs. Metallicity

We have shown in section §4.1 that the MW simulation yields vertical trends in metallicity and rotational velocity similar to those found in SDSS observations presented in I08 & B10. SDSS data also revealed a surprising lack of correlation between V_ϕ and $[\text{Fe}/\text{H}]$, contrary to

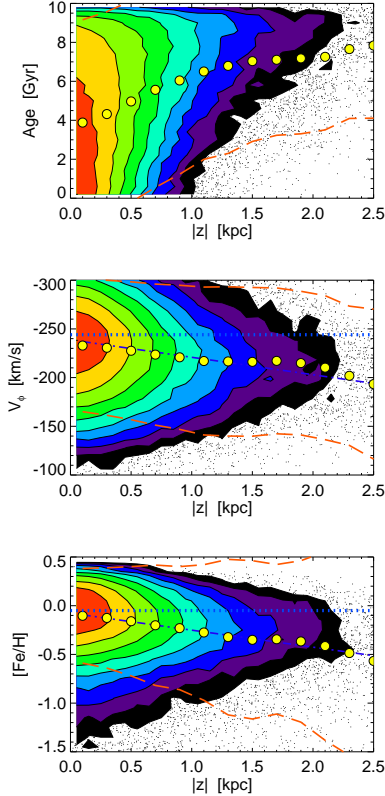


Figure 7. The behavior of $\sim 200,000$ model particles selected from a galactocentric cylindrical annulus with $7 \text{ kpc} < R < 9 \text{ kpc}$. Age, rotational velocity, and metallicity are shown as a function of height in the top, middle, and bottom panels respectively. The data is represented by color-coded contours (low to medium to high: black to green to red) in the regions of high density, and as individual points otherwise. The large symbols show the weighted mean values in $|z|$ bins, and the dashed lines show a 2σ envelope around the weighted means. The dot-dashed line shows the best linear fit to these means. Overplotted for reference in a dotted blue line is the mean rotational velocity and mean metallicity at $z = 0$ in the MW simulation.

the expectations based on a traditional two-disk model (see Appendix A for a discussion of competing observational claims). In the top left panel of Figure 9, we show V_ϕ vs. $[\text{Fe}/\text{H}]$ for the vertical slice considered above ($|z| = 0.5 - 1.0 \text{ kpc}$) corresponding to the transition between the thick and thin disk in the simulation. The MW simulation also yields a lack of correlation between these quantities: although both rotational velocity and metallicity show vertical gradients, when stars are selected from a thin z slice, velocity and metallicity are not correlated.

We can understand why there is no correlation between V_ϕ and $[\text{Fe}/\text{H}]$ if we consider the thin slice as occupied by an age ensemble that was brought together by radial migration. In this light, we can decompose the sample by age to see how the behavior of each population is modified with time (see top left panel of Figure 8 for the age sub-samples considered).

The top right panel of Figure 9 shows a strong correlation between rotational velocity and metallicity exists for young stars; the gradient is $-29 \text{ km s}^{-1} \text{ dex}^{-1}$. The young stars constitute a small fraction of the overall population in the selected volume (10%) and, as the top right and bottom right panels of Figure 8 illustrate,

young stars have correlated metallicity and formation radius. Thus if a young star has a metallicity different than the surrounding ISM, it must originate from somewhere outside the solar cylinder and be at or near perigalacticon (if $R_g \geq 9 \text{ kpc}$, where R_g is the radius of the stellar guiding center) or at or near apogalacticon (if $R_g \leq 7 \text{ kpc}$); consequently, it will either lead or lag the local standard of rest (LSR).

For increasingly older age bins, the gradient diminishes and ultimately fades away. The bottom left and right panels of Figure 9 show V_ϕ vs. $[\text{Fe}/\text{H}]$ for intermediate ($4 \text{ Gyr} \leq \text{Age} \leq 6 \text{ Gyr}$) and old ($8 \text{ Gyr} \leq \text{Age} \leq 10 \text{ Gyr}$) populations respectively. The intermediate age stars constitute 24% of the stellar population in the thin slice and retain a slight gradient $= -17 \text{ km s}^{-1} \text{ dex}^{-1}$. The oldest stars make up 21% of the stellar population and show a nearly flat/slightly positive slope of $8 \text{ km s}^{-1} \text{ dex}^{-1}$.

The peak in the distribution of intermediate and oldest age star particles is offset to progressively lower metallicity and rotational velocity. The metallicity of intermediate age stars ranges from $-0.5 < [\text{Fe}/\text{H}] < 0.5$ while the metallicity of old stars range from $-1.0 < [\text{Fe}/\text{H}] < 0.0$. We can think of these three age bins as dominating different portions of the overall V_ϕ vs. $[\text{Fe}/\text{H}]$ space, with the space spanned by intermediate and old stars being perpendicular to the peak in the correlation in young stars. Thus, for the data cut into slices of $[\text{Fe}/\text{H}]$, the distributions of V_ϕ are offset relative to one another.

For the highest density contours, the mean value of the oldest stars is $[\text{Fe}/\text{H}] = -0.5$, $V_\phi = -210 \text{ km s}^{-1}$; this is significantly lower than the mean value in the highest density contour of the full age sample $[\text{Fe}/\text{H}] = -0.1$, $V_\phi = -225 \text{ km s}^{-1}$. The full age sample’s peak mean value matches the intermediate age values, which is in turn lower than the peak of the youngest stars $[\text{Fe}/\text{H}] = -0.05$, $V_\phi = -245 \text{ km s}^{-1}$. When the entire population is considered as a whole, the correlations disappears.

Why does the V_ϕ - $[\text{Fe}/\text{H}]$ gradient diminish with increasing age? To understand this, we return to Figure 8 and recall that most of the stars within this thin cut are intermediate to old age, and they did not form within $7 \text{ kpc} \leq R \leq 9 \text{ kpc}$. A range of formation radii corresponds to a range of formation environments; this maps to a range of resulting metallicities for stars of a given old age bin. At the same time, depending on a star’s formation location and subsequent migration and scattering off the disk substructure, it can end up with a range of possible rotational velocities (see bottom left panel, Figure 8). Hence, even a single old age bin samples a wide range of formation environments and rotational velocities resulting from unique dynamical histories, which are not directly correlated.

We stress the significant difference between these results and the traditional double-disk interpretation: in the latter case a correlation between V_ϕ and $[\text{Fe}/\text{H}]$ is expected as one moves from younger, metal rich thin disk population to an older, metal poor, thick disk population. In contrast, here we find that a trend is present in the young stars but absent in the older stars. The trend in the young stars can be easily understood as arising from epicyclic motions of stars with their birth radii imprinted into their metallicities. As migration moves the guiding centers of stars, this metallicity encoding is

erased, and the correlation between V_ϕ and $[\text{Fe}/\text{H}]$ disappears.

4.4. Geneva Copenhagen Survey

As we demonstrated above, we can understand why there is no correlation between V_ϕ and $[\text{Fe}/\text{H}]$ when we decompose the sample by age. Older populations have had more time to radially mix; thus in the older age bins the expected trend disappears. That is, the evolution of the trends shown in Figure 9 is a unique signature of radial mixing taking place in the disk.

We can verify whether this is the case in the solar neighborhood by utilizing observational data taken from the Geneva-Copenhagen Survey (GCS) (Holmberg et al. 2009). The GCS samples a wide range of stellar ages and is reasonably well populated with old stars to make qualitative comparisons to the MW simulation in the plane of the disk. While what we have shown in Figure 9 is the relationship at 0.5-1 kpc above the plane, these trends evolve in the same way as a function of age in the mid-plane.

We have selected the non-binary stars from the GCS and repeated the analysis we presented above. Figure 10 shows the results: the top panel shows that there is no net trend when the sample is considered as a whole. Splitting the sample into two broad age bins (0-4 Gyr and 4-15 Gyr) yields a trend only in the young stars – the correlation is completely absent for the older stars. The evolution of the observed V_ϕ vs. $[\text{Fe}/\text{H}]$ trend in the GCS sample therefore matches our expectations based on the simulation and strongly suggests that the stellar populations in the solar neighborhood have been influenced by radial mixing.

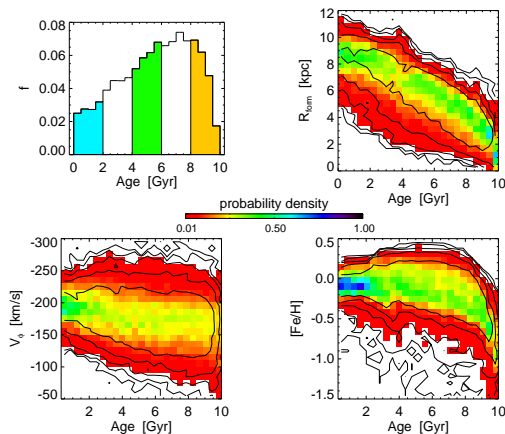


Figure 8. Top left: histogram of stellar ages for subset of data from within thin slice spanning $|z| = 0.5 - 1.0$ kpc, $R = 7 - 9$ kpc; shaded regions correspond to age slices considered in Figure 9. The remaining three panels illustrate probability density maps with logarithmically spaced contours overplotted; here each column sums to 1. Clockwise from top right: formation radius, metallicity, and rotational velocity as a function of age. Note, the top right panel is the same considered in the top right panel in Figure 1.

5. OBSERVATIONAL DECOMPOSITION

We now turn our attention to assigning thin or thick disk membership in a manner analogous to observational studies, i.e. either based on kinematics or metallicity. We

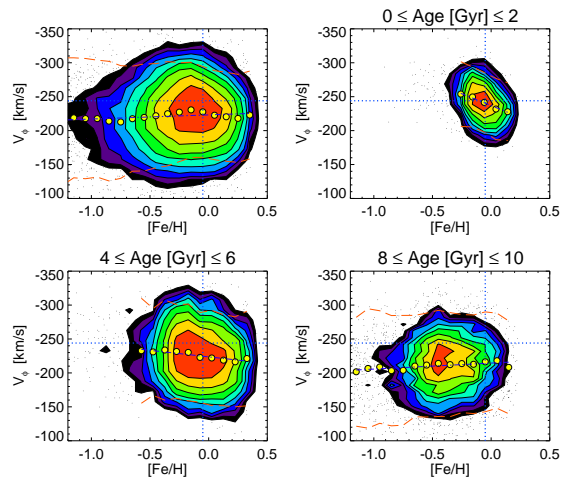


Figure 9. Decomposition of rotational velocity vs. metallicity by age. Top left figure, rotational velocity vs. metallicity for all stars within thin slice $|z| = 0.5 - 1.0$ kpc, $R = 7 - 9$ kpc. Rotational velocity and metallicity are not correlated. Top right, bottom left, and bottom right panels show stars with ages $1, 5, 9$ Gyr ± 1 Gyr respectively. Overplotted for reference with dotted blue lines is the mean rotational velocity and mean metallicity of the gas within the MW simulation’s solar cylinder. As the top left panel of Figure 8 illustrates, the youngest stars are a small fraction of the overall mass distribution; however, these stars show a clear trend of lower metallicity at higher rotational speed. This trend diminishes and eventually disappears for increasingly older stars. Additionally, the mean trend for each age slice is slightly offset; upon superposition, all evidence of any pre-existing trend is erased.

find that classifying stars as members of the thin or thick disk by either velocity or metallicity leads to an apparent separation in the other property, as observed.

5.1. Membership Based on Kinematic Criteria

One of the observational differences between *kinematically selected* thin and thick disk stars is that the latter have higher abundance of α elements at a given $[\text{Fe}/\text{H}]$ (Bensby et al. 2005; Feltzing 2006, and references therein). This difference is often interpreted as evidence for different formation histories. Our simulations include a calculation of the oxygen abundance following the prescription by Raiteri et al. (1999); given that SNII mostly yield oxygen (Hoffman et al. 1999), we use oxygen as a proxy for all α elements. Because metal yields are not precisely known, the normative offset for $[\alpha/\text{Fe}]$ within the MW simulation does not match the Milky Way. However, in terms of chemical evolution, the MW simulation gives a good qualitative perspective on distributions in $[\alpha/\text{Fe}]$ space within the solar cylinder.

The top left panel of Figure 11 shows the overall dependence of $[\alpha/\text{Fe}]$ on $[\text{Fe}/\text{H}]$ for $R = 7 - 9$ kpc, $|z| = 0.0 - 0.3$ kpc (*i.e.* the “solar neighborhood”). A similar behavior is seen for the stars at $|z| \sim 1$ kpc in agreement with Bensby et al. (2005). When the same sample is separated by age, distinct portions of the parameter space are covered. In particular, at low $[\text{Fe}/\text{H}]$, old stars show an enhancement of $[\alpha/\text{Fe}]$ relative to young stars.

Locally, observed thick disk stars are selected kinematically, rather than by age (Prochaska et al. 2000; Reddy et al. 2003, 2006; Allende Prieto et al. 2004). We reproduce the qualitative behavior of observations by following similar steps with the MW simulation. The top right panel in Figure 11 shows a Toomre dia-

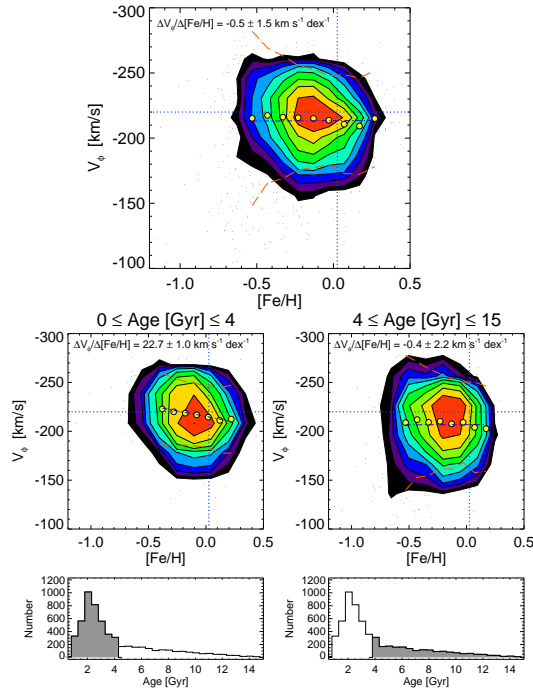


Figure 10. V_ϕ vs. $[\text{Fe}/\text{H}]$ for stars from the Geneva Copenhagen Survey (GCS), which samples stars within 100 pc of the Sun. We have repeated the analysis we presented in Figure 9 for all GCS stars flagged as non-binary. Top panel: when the sample is considered as a whole, there is no discernable trend. Middle row: the sample split into two broad age bins: Age = 0-4 Gyr and Age = 4-15 Gyr. Left middle panel, the young stars show a trend, while in the right middle panel, the old stars are not correlated. This result agrees with the prediction from the MW simulation and strongly motivates a history of radial mixing in the solar neighborhood. Bottom panels: histogram of overall age distribution, with shaded region corresponding to the data sampled in the panel above it.

gram for simulated stars, with selection cuts motivated by Nissen & Schuster (2009). The bottom left panel shows that these kinematically-selected thin and thick disk stars from the solar neighborhood show similar bifurcation of $[\alpha/\text{Fe}]$ vs. $[\text{Fe}/\text{H}]$ behavior as young and old subsamples shown in top left panel. In the bottom right panel, stars from just the shaded $[\text{Fe}/\text{H}]$ cut in the bottom left plot are examined.

Stars falling within the kinematically selected thick disk region have a higher fraction of old stars relative to the overall population. These old stars are α -enhanced as they formed in the interior of the disk and radially migrated to their present location. Thus kinematically dividing the stars locally biases the sample to an older, α -enhanced population. Although the simulation and the data are not in detailed quantitative agreement, these qualitative results imply that the differences in $[\alpha/\text{Fe}]$ vs. $[\text{Fe}/\text{H}]$ for kinematically selected thin and thick disk stars may be another consequence of mixing effects that result from radial migration.

5.2. Membership Based on $[\alpha/\text{Fe}]$ Criteria

Although not as commonly done, it is equally plausible to take the converse approach; we can assign membership to the thin and thick disk based on an $[\alpha/\text{Fe}]$ cut and then study the kinematic and $[\text{Fe}/\text{H}]$ distributions that result (Navarro et al. 2010; Lee et al. 2010). Here we follow the technique outlined by Lee et al. (2010), who chemically

divided the Galactic disks using SDSS SEGUE-1 data; we select star particles within $R = 7 - 11$ kpc, $|z| = 0.3 - 2.0$ kpc and split them so that stars with $[\alpha/\text{Fe}] \geq -0.1$ are assigned thick disk membership.

Assigning membership based on $[\alpha/\text{Fe}]$ effectively divides the disk into two populations: old stars and young – intermediate age stars, as can be seen clearly in the top left panel of Figure 12. Why is this the case? Star particles are born α -enhanced if they form in a region with a high local SFR and little SNIa pollution. Since most old stars originated near the center of the disk, and that region is where the SFR was high, these stars are naturally α -enhanced.

We compare our results to three trends discussed in Lee et al. 2010: the radial metallicity gradient, distribution in V_ϕ and distribution in $[\text{Fe}/\text{H}]$, which we show clockwise from top right in Figure 12. The top right panel illustrates the best fit radial metallicity gradients as derived from the mass weighted mean value of $[\text{Fe}/\text{H}]$. Cutting by $[\alpha/\text{Fe}]$ results in no trend (slope $\sim 0 \text{ kpc dex}^{-1}$) in the thick disk and a negative trend in the thin disk (slope $\sim -0.2 \text{ kpc dex}^{-1}$); this is similar to the thick disk slope = 0 kpc dex^{-1} and thin disk slope = $-0.3 \text{ kpc dex}^{-1}$ observed by Lee et al. (2010). The bottom right panel illustrates the cumulative V_ϕ distributions that result for the MW simulation when stars are separated by $[\alpha/\text{Fe}]$: the thin and thick disk trends are offset by $\sim 25 \text{ km s}^{-1}$, which is qualitatively similar to, if quantitatively smaller than, the $\sim 50 \text{ km s}^{-1}$ offset found by Lee et al. (2010). Finally the bottom left panel shows the cumulative $[\text{Fe}/\text{H}]$ distributions; we find the thin and thick disk trends offset by ~ 0.35 dex, not dissimilar from the observed ~ 0.4 dex offset (Lee et al. 2010).

Therefore, by adopting a kinematic or $[\alpha/\text{Fe}]$ selection criteria used by observers, we are able to reproduce an apparent separation in the other property, despite the fact that there are no distinct populations in the model galaxy.

6. COMPARISON WITH PREVIOUS THEORETICAL WORK

Recently, Schönrich & Binney (2009) investigated how radial migration and chemical evolution shape the solar neighborhood, by incorporating for the first time a prescription for radial migration in a semi-analytic model of Galactic chemical evolution. Their model represented a disk in which star formation commenced at all radii simultaneously (*i.e.* without inside-out growth), with radially varying star formation rates set to yield a disk with an appropriate scale length. The guiding center radii of the stars in their model changed (*i.e.* stars migrated radially) according to a parametrized probabilistic prescription whose normalization was left as a free parameter in the model. The vertical structure of their disk was determined based on the assumption that coeval stars comprise an isothermal population with a velocity dispersion given by local observational constraints. Because stars migrating from the inner disk retain their velocity dispersions but encounter a lower restoring potential in the outer disk, they populate the disk away from the plane. Hence, Schönrich & Binney (2009) showed that a thickened component may result simply by (the inevitable) radial migration, and by fitting the model they also reproduced many of the canonical features of the thick

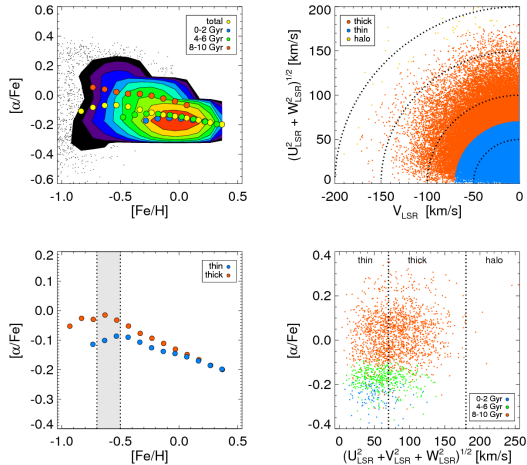


Figure 11. Results of a simple kinematic cut on the local sample: $R = 7 - 9$ kpc, $|z| = 0.0 - 0.3$ kpc. Top left: Distribution of $[\alpha/\text{Fe}]$ for the entire local sample. The distribution is continuous, not bimodal. The mean $[\alpha/\text{Fe}]$ for $[\text{Fe}/\text{H}]$ bins, shown in yellow, qualitatively matches observational data (Bensby et al. 2005). When the sample is decomposed by age, the weighted mean value of old stars is clearly α -enhanced relative to the younger populations. Top right: Toomre diagram. Stars with $V_{\text{LSR}} \geq -70$ km/s are assigned thin disk membership, while stars with $-150 \leq V_{\text{LSR}} < -70$ km/s are considered thick disk. All other stars are assigned halo membership in agreement with Nissen & Schuster (2009). Bottom left: the resulting weighted mean distributions for the thin and thick disk populations. The thick disk is α -enhanced relative to the thin disk at low $[\text{Fe}/\text{H}]$. Bottom right: stars from just the shaded $[\text{Fe}/\text{H}]$ cut in the bottom left plot. Stars falling within the “thick” disk zone have a higher fraction of old stars relative to the overall population. These old stars are α -enhanced. Thus kinematically dividing the stars locally biases the sample to an older, α -enhanced population.

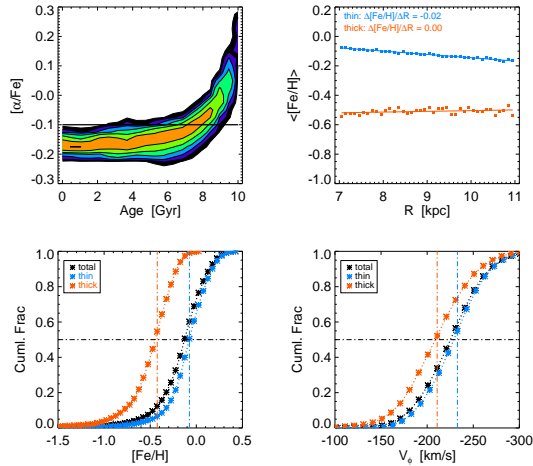


Figure 12. Thin and thick disk membership assigned based on $[\alpha/\text{Fe}]$; the sample includes star particles within $R = 7 - 11$ kpc, $|z| = 0.3 - 2.0$ kpc. Top left: mass weighted contour plot of $[\alpha/\text{Fe}]$ vs. Age in logarithmically spaced bins (low to medium to high: black to green to orange). Overplotted for reference is the dividing line $[\alpha/\text{Fe}] = -0.1$; stars with $[\alpha/\text{Fe}] \geq -0.1$ are considered α -enhanced and are assigned thick disk membership. Clearly the majority of these stars are quite old. Stars with $[\alpha/\text{Fe}] < -0.1$ are considered thin disk members and sample a wide range of ages. Counterclockwise from top right to bottom left: resulting thin and thick disk trends. Notably, the thick disk stars are metal poor with no gradient in R and lag the rotation of the thin disk stars. Despite the appearance of these trends here, there is no distinct thick disk population in the MW simulation.

disk (*i.e.* enhanced $[\alpha/\text{Fe}]$ ratios, older ages, lower metallicities, rotational lag), similar to what we have shown in the previous Section.

It is therefore reassuring that our results presented here agree qualitatively with those of Schönrich & Binney (2009), given that our modeling methods are entirely different, and that our model was not specifically tuned to the Galaxy. However, we also find subtle yet crucial differences. Figure 4 of Schönrich & Binney (2009) shows that due to radial mixing, a population that shares the same kinematics can show immense variations in its chemical composition. The top left panel of Figure 13 shows that our model also yields stellar populations with the same kinematics but very different chemistry, consistent with recent observational work (Navarro et al. 2010). However, we note the contours of mean V_ϕ in this plane are almost orthogonal in our simulation compared to those shown in Fig. 4 of Schönrich & Binney (2009), even though the age structure is very similar; at fixed $[\text{Fe}/\text{H}]$ age increases monotonically with rising $[\alpha/\text{Fe}]$ (middle panel of Figure 13 and Figure 5 of Schönrich & Binney 2009).

A hint of a reason for this discrepancy is provided by scrutinizing the metal-rich end of these figures. In our model, the $[\alpha/\text{Fe}]$ -deficient metal-rich population originated in the interior of the disk (see the rightmost panel of Figure 13) and has migrated to the present radius without very much heating. This is apparent from the fact that the mean V_ϕ for this population is only very slightly lagging the LSR (~ -240 km/s). On the other hand, in the model of Schönrich & Binney (2009), that same population shows considerable lag from the LSR. This discrepancy implies that there are qualitative differences in the treatment of radial mixing between their prescription and our simulation.

On the other hand, the differences in the velocity structure in this plane must also be a result of their assumption that the entire disk begins forming stars at once with a peak in star formation occurring ~ 10 Gyr ago everywhere. In our model, it is impossible to have an old metal poor star which formed at the solar radius - *all* of these stars must have migrated to their present position because the solar neighborhood in our simulation does not exist ~ 9 Gyr ago.

Haywood (2008) argued that the existing solar neighborhood samples (*e.g.* the GCS) show signatures of radial mixing as proposed by Sellwood & Binney (2002). In our sample shown in Figure 13, the metal-poor, low $[\alpha/\text{Fe}]$ stars have high velocities and young ages, and are at or near peri-galactic passage from the outer disk into the solar neighborhood sample. This is consistent with the arguments put forth by Haywood (2008) as observational evidence of radial mixing. However, we point out that the large velocities of this tail in the distribution signify that their orbits have merely been heated, and these stars have not migrated via the corotation scattering mechanism over any significant distance. Instead, it is the presence of significantly metal-enriched stars on kinematically inconspicuous orbits (*i.e.* kinematically cool) that should be considered as clear evidence of migration.

7. PREDICTIONS FOR UPCOMING SURVEYS

We have demonstrated that we can understand the lack of a correlation between V_ϕ and $[\text{Fe}/\text{H}]$ as a consequence

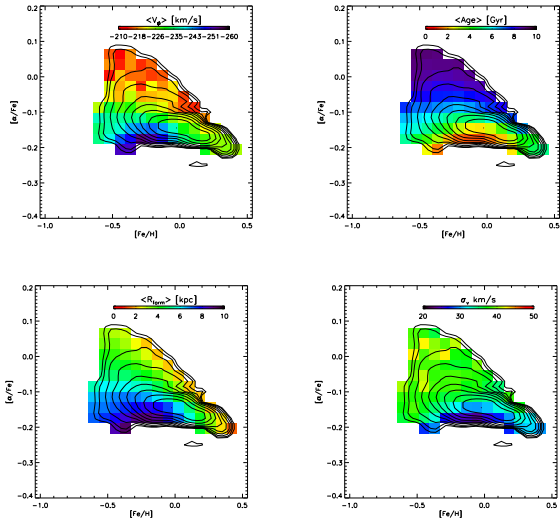


Figure 13. The panels clockwise from top left show distributions of mean V_ϕ , age, σ_V , and R_{form} in the $[\alpha/Fe]$ vs. $[Fe/H]$ plane for particles in the midplane ($|z| < 0.3$ kpc) at the solar radius ($7 < R$ [kpc] < 9). The black contours are logarithmically spaced and indicate particle density, while the colors correspond to the mean of the specified quantity. Only cells containing at least 200 particles are shown.

of radial migration effects; the significance of these effects became clear when we decomposed the MW simulation within the solar cylinder by age. Unfortunately age is not easily accessible observationally. However, α is a directly measurable quantity and, as we have shown, for the oldest stars, α -enhancement is a reasonable proxy for age (see top left panel of Figure 12). Thus we now reassess the relationship between V_ϕ and $[Fe/H]$ by decomposing Figure 9 in cuts of $[\alpha/Fe]$ so that we can make a testable prediction for upcoming observational surveys.

Figure 14 shows V_ϕ vs. $[Fe/H]$ for the “transition zone” considered in Section 4 ($|z| = 0.5 - 1.0$ kpc, $R = 7 - 9$ kpc), as split by two broad bins in $[\alpha/Fe]$. Below each V_ϕ vs. $[Fe/H]$ plot is a histogram of the ages represented in the given bin. In the right panel, the high $[\alpha/Fe]$ sample contains almost exclusively old stars (84% older than 7 Gyr); the corresponding V_ϕ vs. $[Fe/H]$ figure shows no trend between the quantities (best fit slope $\sim 1 \text{ km s}^{-1} \text{ dex}^{-1}$). In contrast to this, the left panel, the low $[\alpha/Fe]$ content bin has few old stars ($< 5\%$ older than 7 Gyr) while sampling young to intermediate aged stars relatively equally (31% between 0 and 2 Gyr old, and 25% between 4 and 6 Gyr old). Here there is a trend between V_ϕ and $[Fe/H]$, with an overall best fit value of $\sim 20 \text{ km s}^{-1} \text{ dex}^{-1}$. We note that this $[\alpha/Fe]$ decomposition works equally well in the solar neighborhood as the “transition zone”.

For the low $[\alpha/Fe]$ cut, we have fit the mass weighted mean values with a single linear fit; however it is equally plausible to fit two lines here: $-0.6 \text{ dex} \leq [\alpha/Fe] \leq -0.2 \text{ dex}$ and the other $-0.2 \text{ dex} \leq [\alpha/Fe] \leq 0.3 \text{ dex}$. In that case, the linear fit to low $[Fe/H]$ shows no trend while the linear fit to high $[Fe/H]$ shows a strong trend. Notably, the portion spanning low $[Fe/H]$ is dominated by the intermediate aged stars while the portion spanning high $[Fe/H]$ is dominated by a younger population. This “knee” is a persistent feature; when the upper limit on

this $[\alpha/Fe]$ cut is lowered, fewer intermediate age stars are sampled, and the knee in the trend shifts to lower $[Fe/H]$. Note, the trend is evident here because on average the stars in this $[Fe/H]$ space have experienced less radial mixing than older stars within the same spatial volume. Thus, it is possible to recover this signature of radial mixing even in the absence of age estimates, but with knowledge of $[\alpha/Fe]$, $[Fe/H]$, and V_ϕ for an unbiased population of stars located out of the midplane.

To date, α measurements have only been accessible to small targeted samples; our initial comparison with a compilation of all currently available data is particularly encouraging (Navarro et al. 2010). We note current work, like that of the SDSS SEGUE collaboration, aims to obtain a large, well-calibrated $[\alpha/Fe]$ dataset. We eagerly anticipate the application of cuts on $[\alpha/Fe]$ to an unbiased population of stars that fall within the region considered by I08 or indeed any large sample within the solar cylinder; such an analysis would further elucidate whether radial mixing has played an important role in shaping the distribution of the Milky Way stars over time.

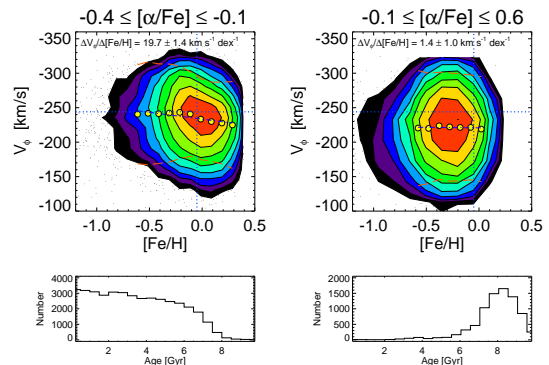


Figure 14. V_ϕ vs. $[Fe/H]$ for two broad bins of $[\alpha/Fe]$ for the volume spanning $|z| = 0.5 - 1.0$ kpc, $R = 7 - 9$ kpc. Top left panel: $-0.4 \leq [\alpha/Fe] \leq -0.1$. Note the knee in the distribution at ~ -0.2 dex. Bottom left panel: the distribution of ages sampled by this $[\alpha/Fe]$ cut. Top and bottom right panel: analogous to the left panel but for $-0.1 \leq [\alpha/Fe] \leq 0.6$. Note the histogram is dominated by stars older than 7 Gyr old and there is no trend in the V_ϕ vs. $[Fe/H]$ figure. This is a clear indication of the importance of radial migration in this volume.

8. CONCLUSIONS

We have used an N-body model designed to mimic the quiescent formation and evolution of a Milky Way-type galactic disk (Roškar et al. 2008ab) to interpret recent SDSS-based observational constraints on the structure of the Milky Way disk. Traditional simplistic decomposition of thin and thick disks as two distinct populations of metallicity and rotational velocity predicts a strong correlation of these quantities at ~ 1 kpc from the Galactic plane. Thanks to nearly complete flux-limited SDSS stellar samples with both rotational and metallicity measurements, the expected correlation was strongly ruled out (Ivezić et al. 2008). On the other hand, the MW simulation we presented here, while not a detailed model of the Milky Way, produces good qualitative agreement with the data and sheds new light on the origin and evolution of the observed disk structure. Of particular im-

portance is the role of radial migration in mixing stars born throughout the disk into the solar neighborhood.

The properties of the Roškar et al. model for the overall spatial, metallicity and kinematic distributions of the Milky Way stars are in qualitative agreement with the SDSS data (Jurić et al. 2008; Ivezić et al. 2008; Bond et al. 2010). While there are quantitative differences in the spatial gradients of these distributions, as well as in their detailed behavior, even this qualitative agreement is remarkable because the simulation was not fine tuned to match the Milky Way. Not only does the model reproduce the observed change of slope in the counts of disk stars as a function of distance from the Galactic plane (the original motivation for introducing a separate thick disk component), but it also predicts the gradients in metallicity and rotational velocity. Furthermore, the metallicity and rotational velocity are uncorrelated in this model for appropriately volume-selected subsamples of stars, in agreement with observations.

The robust qualitative agreements between the data and model predictions motivate the use of model quantities inaccessible to observations, such as the stellar age and the ISM metallicity at the time and position of stellar birth, to interpret recent SDSS results. In particular, the lack of correlation between the metallicity and rotational velocity at ~ 1 kpc from the Galactic plane can be understood as due to complex interplay between the ISM metallicity at the time and position of stellar birth, and the subsequent secular evolution largely driven by spiral arms.

No *a priori* assumptions about the disk's structure are incorporated in the model – yet it reproduces the main observational results which motivated decomposition of the disk into two presumably distinct components. The absence of mergers in this model implies that they are not required to explain the overall disk structure. While merger remnants are detected within the Milky Way disk (e.g. J08), their influence is apparently well localized. Instead, the Milky Way disk can be viewed as a single complex structure with an age distribution that is a strong function of position in the Galaxy due to radial migration of stars. Thus even if a primordial thick disk is present, having formed via accretion/external heating, it is likely to be substantially polluted by migrating disk stars.

The same mixing effects are likely responsible for the observed differences in α element abundance between *kinematically selected* thin and thick disk stars. By adopting kinematic selection criteria used by observers, we are able to reproduce distinctive $[\alpha/\text{Fe}]$ vs. $[\text{Fe}/\text{H}]$ trends similar to those seen in the data, despite the fact that there are no distinct populations in the model galaxy.

We look forward to the improved data derived from the emerging generation of surveys such as SEGUE (Rockosi et al. 2009) and APOGEE (Majewski et al. 2010). Key to garnering a deeper understanding of the importance of radial migration in the Milky Way evolution is gathering both precise age determinations and detailed chemical compositions. We are optimistic that this study will lead to further observational and theoretical work.

9. ACKNOWLEDGMENTS

We thank our numerous SDSS (www.sdss.org) collaborators for their valuable contributions and helpful discussions. S. Loebman and Ž. Ivezić acknowledge support by NSF grants AST-0707901 and AST-1008784 to the University of Washington, and by NSF grant AST-0551161 to LSST for design and development activity. Ž. Ivezić acknowledges support by the Croatian National Science Foundation grant O-1548-2009. This research was supported in part by the NSF through TeraGrid resources provided by TACC and PSC. R. Roškar and T. R. Quinn were supported by the NSF ITR grant PHY-0205413 at the University of Washington.

REFERENCES

- Abadi, M. G., Navarro, J. F., Steinmetz, M., & Eke, V. R. 2003, *Astroph. J.*, 597, 21
- Abe, F., et al. 1999, *Astron. J.*, 118, 261
- Allende Prieto, C., Barklem, P. S., Lambert, D. L., & Cunha, K. 2004, *VizieR Online Data Catalog*, 342, 183
- Bahcall, J. N., & Soneira, R. M. 1980, *ApJ*, 238, L17
- Bensby, T., Feltzing, S., & Lundström, I. 2003, *A&A*, 410, 527
- Bensby, T., Feltzing, S., Lundström, I., & Ilyin, I. 2005, *A&A*, 433, 185
- Binney, J. 2010, *MNRAS*, 401, 2318
- Bochanski, J. J., Munn, J. A., Hawley, S. L., West, A. A., Covey, K. R., & Schneider, D. P. 2007, *Astron. J.*, 134, 2418
- Bond, N. A., et al. 2010, *Astroph. J.*, 716, 1
- Bournaud, F., Elmegreen, B. G., & Martig, M. 2009, *ApJ*, 707, L1
- Brewer, M. M. 2004, Ph.D. thesis, The University of North Carolina at Chapel Hill
- Brook, C. B., Gibson, B. K., Martel, H., & Kawata, D. 2005, *Astroph. J.*, 630, 298
- Brook, C. B., Kawata, D., Gibson, B. K., & Freeman, K. C. 2004, *Astroph. J.*, 612, 894
- Bullock, J. S., Dekel, A., Kolatt, T. S., Kravtsov, A. V., Klypin, A. A., Porciani, C., & Primack, J. R. 2001, *Astroph. J.*, 555, 240
- Bullock, J. S., & Johnston, K. V. 2005, *Astroph. J.*, 635, 931
- Burstein, D. 1979, *Astroph. J.*, 234, 829
- Buser, R., Rong, J., & Karaali, S. 1999, *A&A*, 348, 98
- Carollo, D., et al. 2010, *Astroph. J.*, 712, 692
- Caruana, J. 2009, Dissertation bsc (hons), Department of Physics, University of Malta
- Chen, B., et al. 2001, *Astroph. J.*, 553, 184
- Chiba, M., & Beers, T. C. 2000, *Astron. J.*, 119, 2843
- Dierickx, M., Klement, R. J., Rix, H., & Liu, C. 2010, *ArXiv e-prints*
- Feltzing, S. 2006, *Memorie della Societa Astronomica Italiana*, 77, 1103
- Feltzing, S., Bensby, T., & Lundström, I. 2003, *A&A*, 397, L1
- Fuhrmann, K. 1998, *A&A*, 338, 161
- Gilmore, G., & Reid, N. 1983, *MNRAS*, 202, 1025
- Gilmore, G., Wyse, R. F. G., & Norris, J. E. 2002, *ApJ*, 574, L39
- Haywood, M. 2008, *MNRAS*, 388, 1175
- Hoffman, R. D., Woosley, S. E., Weaver, T. A., Rauscher, T., & Thielemann, F. 1999, *Astroph. J.*, 521, 735
- Holmberg, J., Nordström, B., & Andersen, J. 2009, *A&A*, 501, 941
- Ivezić, Ž., et al. 2008, *Astroph. J.*, 684, 287
- Jones, B. J. T., & Wyse, R. F. G. 1983, *A&A*, 120, 165
- Jurić, M., et al. 2008, *Astroph. J.*, 673, 864
- Kaufmann, T., Mayer, L., Wadsley, J., Stadel, J., & Moore, B. 2007, *MNRAS*, 375, 53
- Kazantzidis, S., Bullock, J. S., Zentner, A. R., Kravtsov, A. V., & Moustakas, L. A. 2008, *Astroph. J.*, 688, 254
- Larsen, J. A., & Humphreys, R. M. 2003, *Astron. J.*, 125, 1958
- Lee, Y. S., et al. 2010, in *Bulletin of the American Astronomical Society*, Vol. 41, *Bulletin of the American Astronomical Society*, 250
- Loebman, S., et al. 2008, in *American Institute of Physics Conference Series*, Vol. 1082, *American Institute of Physics Conference Series*, ed. C. A. L. Bailer-Jones, 238
- Majewski, S. R. 1993, *ARA&A*, 31, 575

- Majewski, S. R., Wilson, J. C., Hearty, F., Schiavon, R. R., & Skrutskie, M. F. 2010, in IAU Symposium, Vol. 265, IAU Symposium, ed. K. Cunha, M. Spite, & B. Barbuy, 480
- Mishenina, T. V., Soubiran, C., Kovtyukh, V. V., & Korotin, S. A. 2004, A&A, 418, 551
- Munn, J. A., et al. 2004, Astron. J., 127, 3034
- Navarro, J. F., Abadi, M. G., Venn, K. A., & Freeman, K. C. 2010, ArXiv e-prints
- Navarro, J. F., Frenk, C. S., & White, S. D. M. 1997, Astroph. J., 490, 493
- Neeser, M. J., Sackett, P. D., De Marchi, G., & Paresce, F. 2002, A&A, 383, 472
- Nissen, P. E. 1995, in IAU Symposium, Vol. 164, Stellar Populations, ed. P. C. van der Kruit & G. Gilmore, 109
- Nissen, P. E., & Schuster, W. J. 2009, in IAU Symposium, Vol. 254, IAU Symposium, ed. J. Andersen, J. Bland-Hawthorn, & B. Nordström, 103
- Norris, J. E. 1999, Ap&SS, 265, 213
- Ojha, D. K. 2001, MNRAS, 322, 426
- Parker, J. E., Humphreys, R. M., & Beers, T. C. 2004, Astron. J., 127, 1567
- Prochaska, J. X., Naumov, S. O., Carney, B. W., McWilliam, A., & Wolfe, A. M. 2000, Astron. J., 120, 2513
- Quinn, P. J., Hernquist, L., & Fullagar, D. P. 1993, Astroph. J., 403, 74
- Raiteri, C. M., Villata, M., Gallino, R., Busso, M., & Cravanzola, A. 1999, ApJ, 518, L91
- Reddy, B. E., Lambert, D. L., & Allende Prieto, C. 2006, MNRAS, 367, 1329
- Reddy, B. E., Tomkin, J., Lambert, D. L., & Allende Prieto, C. 2003, MNRAS, 340, 304
- Robin, A. C., Haywood, M., Creze, M., Ojha, D. K., & Bienayme, O. 1996, A&A, 305, 125
- Rockosi, C., Beers, T. C., Majewski, S., Schiavon, R., & Eisenstein, D. 2009, in Astronomy, Vol. 2010, astro2010: The Astronomy and Astrophysics Decadal Survey, 14
- Roškar, R., Debattista, V. P., Quinn, T. R., Stinson, G. S., & Wadsley, J. 2008a, ApJ, 684, L79
- Roškar, R., Debattista, V. P., Stinson, G. S., Quinn, T. R., Kaufmann, T., & Wadsley, J. 2008b, ApJ, 675, L65
- Ruchti, G. R., et al. 2010, ArXiv e-prints
- Sales, L. V., et al. 2009, MNRAS, 400, L61
- Schönrich, R., & Binney, J. 2009, MNRAS, 396, 203
- Sellwood, J. A., & Binney, J. J. 2002, MNRAS, 336, 785
- Sesar, B., Ivezić, Ž., & Jurić, M. 2008, Astroph. J., 689, 1244
- Shen, S., Wadsley, J., & Stinson, G. 2009, ArXiv e-prints, 0910.5956
- Siegel, M. H., Majewski, S. R., Reid, I. N., & Thompson, I. B. 2002, Astroph. J., 578, 151
- Smagorinsky, J. 1963, Monthly Weather Review, 91, 99
- Soubiran, C., Bienaymé, O., & Siebert, A. 2003, A&A, 398, 141
- Spagna, A., Lattanzi, M. G., Re Fiorentin, P., & Smart, R. L. 2010, A&A, 510, L4
- Spitzer, L., Jr. 1942, Astroph. J., 95, 329
- Statler, T. S. 1988, Astroph. J., 331, 71
- Steinmetz, M., et al. 2006, Astron. J., 132, 1645
- Stinson, G., Seth, A., Katz, N., Wadsley, J., Governato, F., & Quinn, T. 2006, MNRAS, 373, 1074
- Tautvaišienė, G., Edvardsson, B., Tuominen, I., & Ilyin, I. 2001, A&A, 380, 578
- van der Kruit, P. C., & Searle, L. 1981, A&A, 95, 105
- Villalobos, Á., & Helmi, A. 2008, MNRAS, 391, 1806
- Villalobos, Á., Kazantidis, S., & Helmi, A. 2010, Astroph. J., 718, 314
- Wadsley, J. W., Stadel, J., & Quinn, T. 2004, New Astronomy, 9, 137
- Wadsley, J. W., Veeravalli, G., & Couchman, H. M. P. 2008, MNRAS, 387, 427
- Wilson, M., et al. 2010, ArXiv e-prints
- Wyse, R. F. G., Gilmore, G., Norris, J. E., Wilkinson, M. I., Kleyna, J. T., Koch, A., Evans, N. W., & Grebel, E. K. 2006, ApJ, 639, L13
- Yoachim, P. 2007, Ph.D. thesis, University of Washington
- Yoachim, P., & Dalcanton, J. J. 2005, Astroph. J., 624, 701
- Yoachim, P., & Dalcanton, J. J. 2006, Astron. J., 131, 226
- Zolotov, A., Willman, B., Brooks, A. M., Governato, F., Brook, C. B., Hogg, D. W., Quinn, T., & Stinson, G. 2009, Astroph. J., 702, 1058

APPENDIX

CONFLICTING OBSERVATIONAL CLAIMS

Recently, Spagna et al. (2010) found that the rotational velocity for disk stars is correlated with metallicity for $-1 < [\text{Fe}/\text{H}] < -0.5$ at $1 \text{ kpc} < z < 3 \text{ kpc}$. Notably, they found a gradient within $40 - 50 \text{ km s}^{-1} \text{ dex}^{-1}$, such that more metal-poor stars rotate more slowly. Their claim is in direct conflict with several other observational studies (Carollo et al. 2010, I08, B10).

We reconsider the Spagna et al. (2010) findings using SDSS DR7 data to try to understand the differences between these observational findings. We note a direct comparison between I08 and Spagna et al. (2010) is non-trivial as Spagna et al. (2010) use their own proper motion measurements based on the GSC-II catalog and do not provide a comparison to the Munn et al. (2004) proper motions on a star-by-star basis. Additionally, their color selection is more generous ($0.0 < g - r < 0.9$) than previous studies ($0.2 < g - r < 0.6$, I08). This more generous selection lets in BHB stars, as well as red stars where $[\text{Fe}/\text{H}]$ reliability decreases. Despite differences in selection criteria, we can reproduce Spagna et al. (2010) results when using the SDSS *spectroscopic* sample (see left panel, Figure 15).

While the left panel of Figure 15 only considers a narrow bin of $z = 1.0 - 1.5 \text{ kpc}$, we find the best fit lines are reproducible for other bins as well. Notably, the median V_ϕ as a function of $[\text{Fe}/\text{H}]$ closely follows the Spagna et al. (2010) result. We also reproduce a bimodal distribution of stars in the metallicity direction, with modes at $[\text{Fe}/\text{H}] \sim -0.65$ and $[\text{Fe}/\text{H}] \sim -0.4$ (see Section 3.2, Spagna et al. 2010).

However, we detect no $V_\phi - [\text{Fe}/\text{H}]$ correlation when we consider a complete sample selected in the meridional plane ($l \sim 0^\circ$ or $l \sim 180^\circ$), where proper motion alone suffices to measure rotational velocity (see right panel, Figure 15). This sample is essentially complete in selected color-distance limits and thus not subject to strong selection effects present in the SDSS spectroscopic sample. This sample shows negligible dependence of the median V_ϕ on $[\text{Fe}/\text{H}]$ for $[\text{Fe}/\text{H}] > -1.0$ (one can also see the bias due to halo stars for $[\text{Fe}/\text{H}] < -1.0$).

It is highly likely that the Spagna et al. (2010) results are caused by selection biases in the SDSS spectroscopic sample. Notably, when we fit two gaussians (one for the disk and halo) to the V_ϕ and $[\text{Fe}/\text{H}]$ distributions, about 45% of the spectroscopic sample are halo stars (consistent with Spagna et al. (2010) within $\sim 5\%$ errors), while halo stars make up only 8% of the complete sample. And when we compare the two panels in Figure 15 we are using exactly the same volume and exactly the same measurements: the only difference between the samples is that the spectroscopic sample includes only $\sim 2\%$ of all the stars, with the selection probability about 10 times higher for halo stars than for disk stars.

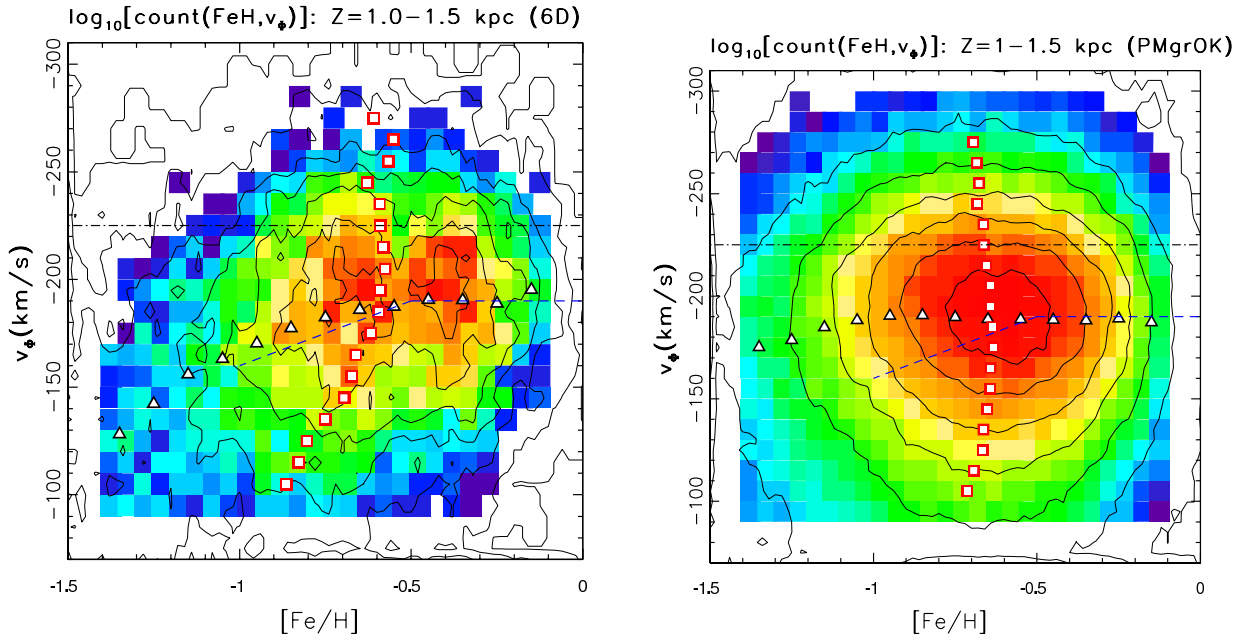


Figure 15. Left panel: $\sim 16,000$ stars selected from SDSS DR7 spectroscopic sample with $g - r = 0.2 - 0.6$ from $z = 1.0 - 1.5$ kpc. The stellar number density is shown as the color-coded map (low to high: blue to red) and by the contours. Triangles are the median V_ϕ for bins of $[\text{Fe}/\text{H}]$, and squares are the median $[\text{Fe}/\text{H}]$ for bins of V_ϕ . Spagna et al. (2010) results are overplotted with a dashed blue line for reference. Right panel: Analogous to plot in right panel but for full photometric sample: $\sim 124,000$ stars with $g - r = 0.2 - 0.6$ and $z = 1.0 - 1.5$ kpc, selected from the meridional plane defined by $l \sim 0^\circ$ or $l \sim 180^\circ$ (See Section 3.2 in Bond et al. 2010).